Supplement of The Cryosphere, 19, 1995–2015, 2025
https://doi.org/10.5194/tc-19-1995-2025-supplement

The Cryosphere Open Access EGU

Supplement of

Importance of ice elasticity in simulating tide-induced grounding line variations along prograde bed slopes

Natalya Ross et al.

Correspondence to: Natalya Ross (nmaslenn@cougarnet.uh.edu)

S.1. Reference measurements

Grounding zone measurements were performed using pairs of DInSAR interferograms at high and low tide; bedrock slope and ice thickness were calculated using Bed Machine Antarctica, and ice flow speed was determined using MEaSUREs InSAR-based ice velocity map of Antarctica (Rignot et al., 2017). The summary of the measurements, performed along ~20 km-long flow lines (see Figure 1), are provided in Table S1.

Table S1. Minimum, maximum, and average values of the grounding zone width, ice thicknesses, bed slopes, and ice flow speed of TOT, MU, and REN glaciers calculated along the profiles of the corresponding glaciers.

Glacier characteristics		TOT	MU	REN	Data source
Grounding zone, km	Min	1.2 ±0.4	0.6 ±0.4	1.3±0.4	Pairs of DInSAR interferograms
	Mean	4.1±0.4	2.1±0.4	2.3±0.4	
	Max	14.9±0.4	5.1±0.4	3.4±0.4	
Ice thickness, km	Min	1.9±0.2	2.0±0.2	0.9±0.3	BedMachine2 (Morlighem et al., 2017)
	Mean	2.2±0.1	2.2±0.1	1.1±0.2	
	Max	2.4±0.2	2.4±0.1	1.2±0.1	
Bed slope, %	Min	0.01±0.01	0.2±0.2	0.3±0.2	BedMachine2 (Morlighem et al., 2017)
	Mean	1.2±0.1	2.2±0.2	1.4±0.2	
	Max	4.0±0.2	5.9±0.3	3.5±0.3	
Ice flow speed, m / year	Min	492 ±113	171±41	117±51	InSAR-based ice velocity data provided by MEaSUREs program (Rignot et al., 2017).
	Mean	647±65	335 ±20	172±24	
	Max	754±49	381±18	192±12	

S.2. Tidal and IBE effects

Tidal heights during satellite passages and Inverse barometer effect (IBE) correction values for each interferogram are provided in Table S2. The tidal heights were estimated using the Circum-Antarctic Tidal Simulation (CATS2008) (Padman et al., 2002), while the IBE correction values were obtained using ERA-5 (Hersbach et al., 2020).

Table S2. Differences in tidal levels for the pairs of DInSAR interferograms after accounting for the IBE correction. The acquisition dates of the Primary 1 (P_1), Secondary 1 (S_1), Primary 2 (P_2), and Secondary 2 (S_2) images are shown in YYYYMMDD format. The values are provided in meters. The differential tidal difference (∆Tide) shows the tidal variation within one interferogram and is calculated as the difference between the tidal levels of the image pairs: $\Delta\ Tide\ =\ (Tide\ (P_1)\ -\ Tide(S_1))\ -\ (Tide\ (P_2)\ -\ Tide\ (S_2))$. The differential IBE correction was calculated similarly. H correspond to the maximum tidal height after applying the IBE correction (H = Max tide + ∆IBE). ∆H shows the difference in corrected maximum tidal levels between the pairs of interferograms for each glacier.

Glacier	P_1	S_1	P_2	S_2	Tide P_1	Tide S_1	Tide P_2	Tide S_2	∆ Tide	Max tide	IBE P_1	IBE S_1	IBE P_2	IBE S_2	∆ IBE	∆ Tide + ∆ IBE	H	∆ H
TOT	20201015	20201016	20201116	20201117	0.45	0.23	-0.53	-0.61	0.14	0.45	0.25	0.11	0.44	0.38	0.08	0.22	0.53	1.03
TOT	20201116	20201117	20201202	20201203	-0.53	-0.61	-0.48	-0.55	0.01	-0.48	0.44	0.38	0.27	0.19	-0.02	-0.01	-0.5	
REN	20201010	20201011	20201111	20201112	-0.09	-0.14	0.83	0.96	0.18	0.96	0.43	0.15	0.38	0.28	0.18	0.36	1.14	1.08
REN	20201010	20201011	20201213	20201214	-0.09	-0.14	-0.16	-0.02	0.19	-0.02	0.43	0.15	0.41	0.21	0.08	0.27	0.06	
MU	20210503	20210504	20210706	20210707	0.76	0.48	-0.21	-0.13	0.36	0.76	0.21	0.16	0.28	0.32	0.09	0.45	0.85	0.95
MU	20210604	20210605	20210706	20210707	-0.15	-0.24	-0.21	-0.13	0.17	-0.13	0.17	0.18	0.28	0.32	0.03	0.2	-0.1	

S.3. Model notation

The notation used in this paper is listed in Table S3.

Table S3. Models' principal notation.

Symbol	Quantity	Field type	Units
	Geometry-related quantities		
$(\boldsymbol{X}, \boldsymbol{Y})$	laboratory coordinate system	2D coordinate system	(m, m)
$\boldsymbol{x} = (\boldsymbol{x}, \boldsymbol{y})$	spatial point $\boldsymbol{x}$ with coordinates x and y	Point in 2D space	(m, m)
$\boldsymbol{\Omega}$	2D glacier domain	2D spatial domain	(m, m)
$\boldsymbol{\partial\Omega}$	boundary of the glacier domain	Geometric boundary	m
$\boldsymbol{\Gamma_D}$	inflow boundary	Geometric boundary	m
$\boldsymbol{\Gamma_N}$	outflow boundary	Geometric boundary	m
$\boldsymbol{\Gamma_a}$	ice–air surface	Geometric boundary	m
$\boldsymbol{\Gamma_b}$	ice–bedrock surface	Geometric boundary	m
$\boldsymbol{\Gamma_w}$	ice–water surface	Geometric boundary	m
$\boldsymbol{\Gamma_s}$	lower glacier boundary	Geometric boundary	m
$\boldsymbol{h(x,t)}$	surface elevation of the ice shelf	Scalar	m
$\boldsymbol{s(x,t)}$	lower boundary of the ice shelf	Scalar	m
$\boldsymbol{\alpha}$	bedrock slope	Scalar	%
$\boldsymbol{b(x)}$	bedrock slope function	Scalar	m
$\boldsymbol{A}$	bedrock inclination parameter	Scalar	m
$\boldsymbol{L}$	glacier length	Scalar	m
$\boldsymbol{H(t)}$	glacier thickness	Scalar	m
$\boldsymbol{l(t)}$	sea level	Scalar	m
$\hat{\boldsymbol{n}}(\boldsymbol{x})$	unit outward normal vector at point $\boldsymbol{x}$ of a domain boundary	Vector	$-$
	Materials properties		
$\boldsymbol{\rho_i}$	ice density	Scalar	$kg \cdot m^{-3}$
$\boldsymbol{\rho_w}$	water density	Scalar	$kg \cdot m^{-3}$
$\boldsymbol{\phi}$	friction	Scalar	$Pa \cdot s \cdot m^{-1}$
$\boldsymbol{C}$	friction coefficient	Scalar	$Pa \cdot \left(\frac{s}{m}\right)^{\frac{1}{n}}$
$\boldsymbol{\eta}$	ice viscosity	Scalar	$Pa \cdot s$
$\boldsymbol{G}$	shear modulus	Scalar	Pa
$\boldsymbol{\lambda}$	relaxation time	Scalar	s
$\boldsymbol{n}$	stress exponent (from the Glen's flow law)	Scalar	$-$
$\boldsymbol{A}$	ice softness	Scalar	$Pa^{-n} \cdot s^{-1}$
	Physical quantities		
$\boldsymbol{t}$	time	Scalar	s
$\boldsymbol{p}$	ice pressure	Scalar	Pa
$\boldsymbol{p_w}$	water pressure at the ice–water interface	Scalar	Pa
$\boldsymbol{p_w^0}$	hydrostatic water pressure	Scalar	Pa
$\boldsymbol{v_0}$	inflow speed on Γ_D	Scalar	$m \cdot s^{-1}$
$\boldsymbol{v}$	ice flow velocity	Vector	$m \cdot s^{-1}$

$\boldsymbol{g}$	acceleration due to gravity	Vector	$m \cdot s^{-2}$
$\boldsymbol{D}$	strain rate tensor	Tensor	s^{-1}
$\boldsymbol{T}$	Cauchy stress tensor	Tensor	Pa
$\boldsymbol{\tau}$	deviatoric stress tensor	Tensor	Pa
	Mathematical operators		
$\mathbb{I}$	identity tensor	Tensor	$-$
$\mathbb{P}$	orthogonal projection onto the boundary	Tensor	$-$
$\boldsymbol{\nabla}$	spatial gradient operator	Operator	m^{-1}
$\boldsymbol{\nabla} \cdot$	spatial divergence operator	Operator	m^{-1}
$\cdot$	inner (dot) product	Operator	$-$
$\otimes$	tensor product	Operator	$-$
$\overset{\nabla}{\boldsymbol{\tau}}$	upper-convected time derivative of some tensor field (in this case, of the tensor $\boldsymbol{\tau}$)	Operator	$Pa \cdot s^{-1}$
	Model numerical parameters		
$\boldsymbol{\delta} \ll \mathbf{1}$	Glen's flow law numerical parameter, used to prevent model numerical instabilities	Scalar	s^{-2}
$\boldsymbol{\varepsilon} \ll \mathbf{1}$	Numerical parameter in the friction expression, used to prevent numerical instabilities	Scalar	$m^2 \cdot s^{-2}$

S.4. Comparison of viscous and viscoelastic models

Short comparison of the main aspect of the models, including the computational time to run each model for different input parameters is provided in Table S4.

Table S4. Comparison of the main properties of the viscous and viscoelastic models.

Characteristics		Viscous model	Viscoelastic model	Similarity
Material properties of glacier flow				
Compressibility		Incompressible	Incompressible	Same
Rheological behavior		Non-Newtonian	Non-Newtonian	Same
Material behavior		Viscous	Viscoelastic	Different
Physical formulation of the models				
Glacier domain		Equations (1) – (5)	Equations (1) – (5)	Same
Boundary conditions		Equations (22) – (27)	Equations (22) – (27)	Same
Governing equation	Conservation of mass in case of incompressibility	Equation (6)	Equation (6)	Same
	Conservation of momentum (Stokes equation)	Equation (7)	Equation (7)	Same
	Constitutive law (Hooke's law)	Both Hooke's law (8) and ice viscosity (10) are defined via strain rate tensor (9)	Both Hooke's law (11) and ice viscosity (13) are defined via deviatoric stress tensor τ (12), which, in turn, depends on strain rate tensor (9)	Different
Implementation of the models				
Penalized problem solved by the model on each time step		Equation (3.21) in (Stubblefield et al., 2021)	Equation (40)	Different
Computation time* (HH:MM:SS)	Glacier thickness = 1.0 km	01:07:07	02:57:48	Different
	Glacier thickness = 1.5 km	01:34:29	04:21:10	Different
	Glacier thickness = 2.0 km	01:59:54	06:07:50	Different
	Glacier thickness = 2.5 km	02:41:39	07:30:08	Different

* For 2.3 GHz 8-Core Intel Core i9 processor. Model input parameters: Domain length = 20 km; Bed slope = 1.0 %; Inflow speed = 100 m/year; Mesh size = 250 m and 50 m on upper and lower domain boundaries, respectively. The time is provided the HH:MM:SS format, where H shows the number of hours, M shows the number of minutes, and S is the number of seconds

S.5. Mesh sensitivity analysis

Models' sensitivity to mesh size was analyzed using 200 grounding zone width values Figure S1), obtained for different mesh sizes of the lower domain surface (from 10 m to 250 m with 10 m step) and constant mesh size of 250 m at the upper domain surface. Through multiple models runs, we determined that reducing the mesh size on the upper boundary does not enhance the results but significantly increases computational time. For both models, the tests were performed for four sets of input parameters: 1) bed slope of 0.5 %, glacier thickness of 1 km, and ice inflow speed of 100 m/year (green dots in Figure S1); 2) bed slope of 5 %, glacier thickness of 1 km, and ice inflow speed of 100 m/year (red dots in Figure S1); 3) bed slope of 5 %, glacier thickness of 2.5 km, and ice inflow speed of 100 m/year (blue dots in Figure S1); 4) bed slope of 5 %, glacier thickness of 1 km, and ice inflow speed of 800 m/year (black dots in Figure S1). The viscoelastic model is more affected by mesh size than the viscous model. For example, grounding zone width values for glaciers with thicknesses of 2.5 km and 1 km, both with an inflow speed of 100 m/year, converge to approximately 1.45 km for a mesh size of 250 m. However, at a mesh size of 10 m, these values were 0.96 km and 0.84 km, respectively (Figure S1 (d)). Comparing the dependences for the same slope of 5% for both models, we conclude that for glaciers with the same thickness, lower ice flow speed is mere sensitive to the mesh size (red and black dots in Figure S1 (c) and (d)).

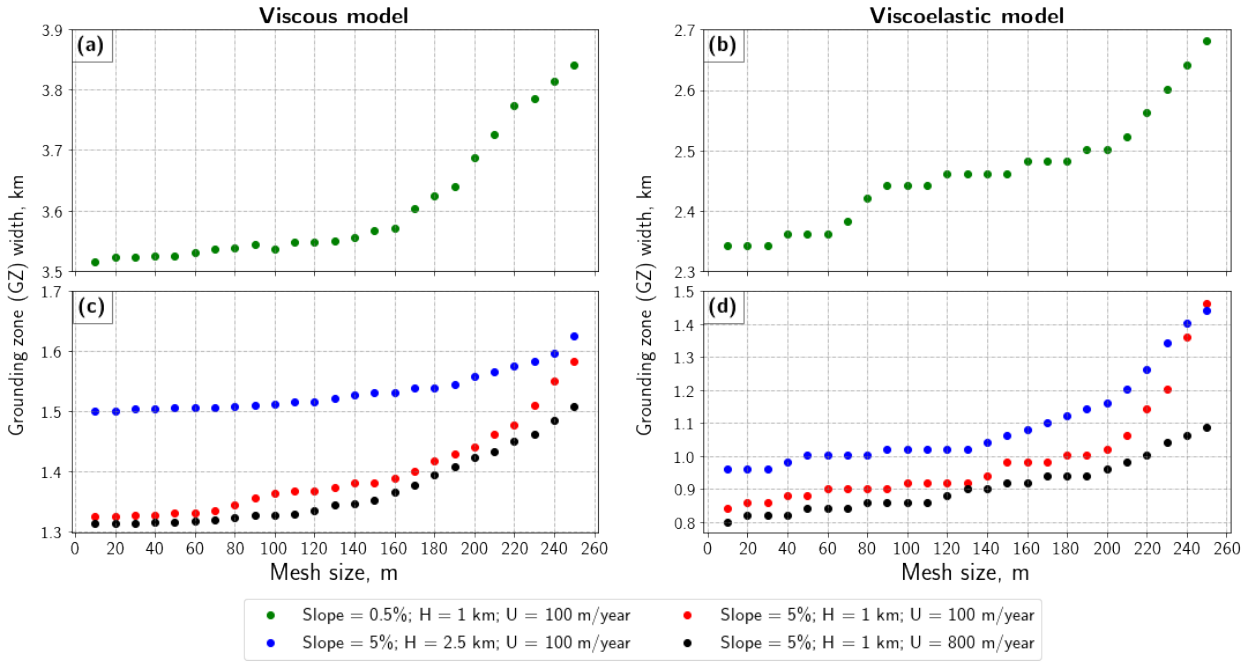

Figure S1. Models mesh sensitivity check. Plots (a) and (c) correspond to the viscous model, and plots marked (b) and (d) represent the viscoelastic model.

S.6. DInSAR data-inferred parameters as model inputs

Fixing 50 m and 250 m as mesh sizes at the lower and upper domain boundaries, respectively, and keeping the constant glacier domain length of 20 km, each model was executed 192 times using all possible combinations of input parameters, listed in Figure S2.

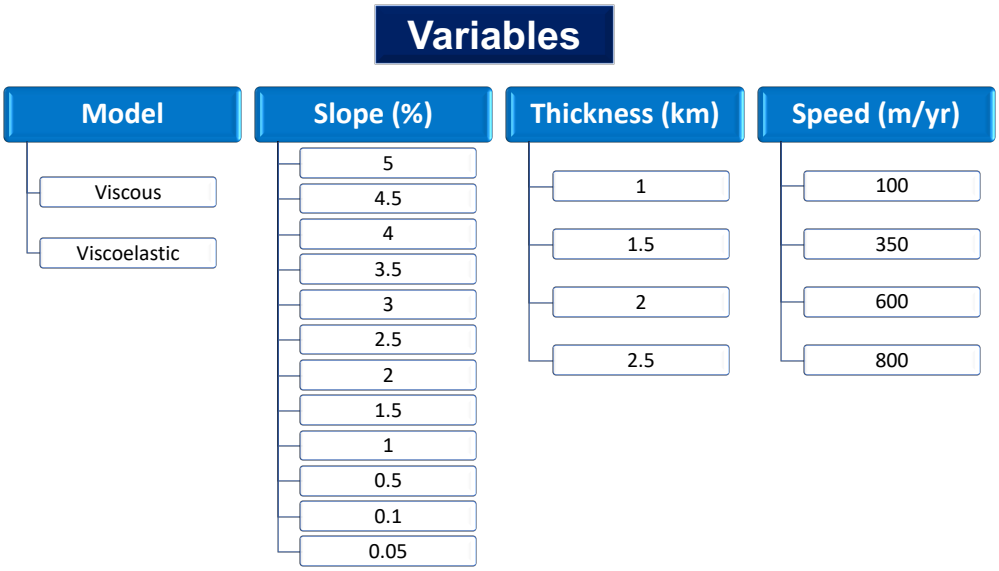

Figure S2. Schematic representation of the initial parameters. All possible combinations of these variables were examined in the paper.

S.7. Reference relationship between bed slopes and grounding zones

The measured grounding zones correlate with bed slopes as an inverse power law, shown in Figure S3.

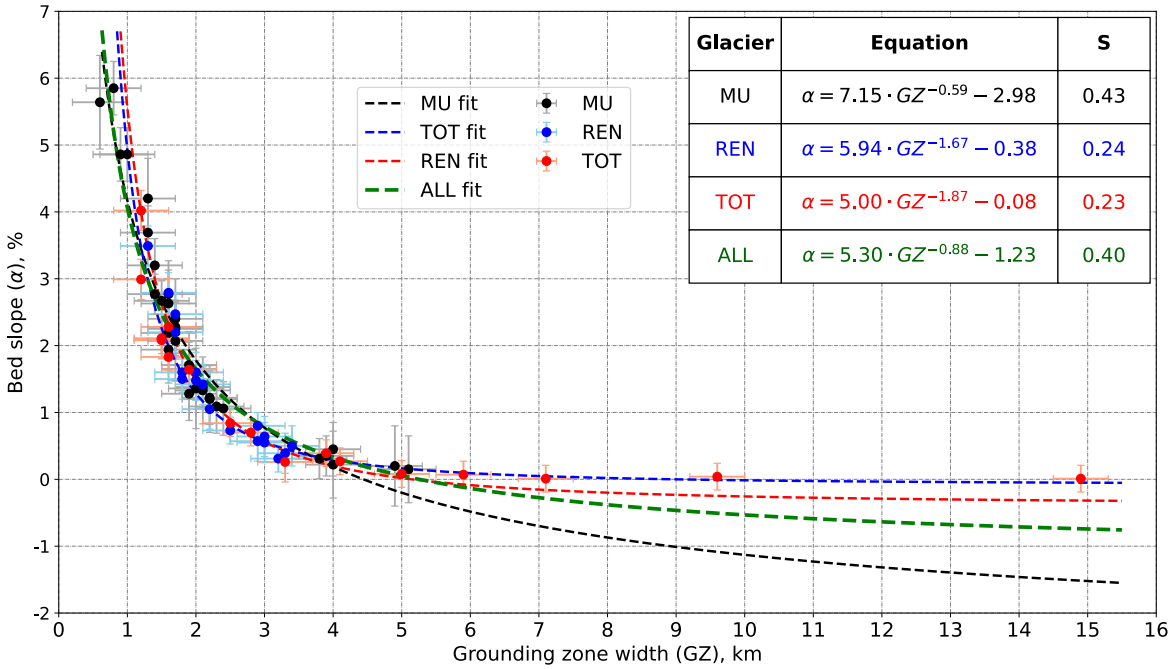

Figure S3. Correlation between DInSAR-derived grounding zones (GZ) and bedrock slopes (α). The measurements were approximated using an inverse power law function $\alpha = a \cdot GZ^b + c$, where $b < 0$. The fit quality was evaluated using standard error of regression (S) and is shown in the table in the top right corner alongside the corresponding approximating equations.

S.8. Grounding zone evolution with glacier thickness

The dependence of grounding zone width (GZ) on glacier thickness (H) for each inflow speed and bed slope, approximated with a linear function $GZ = a \cdot H + b$, provides unique coefficients a and b for each model formulation, bed slope, and ice inflow speed. These a and b values are listed in Table S5.

Table S5. Equations of the approximating lines of all considered dependences of the grounding zone magnitude from the glacier thickness.

Slope, %	Inflow speed, m/year	Approximating line equation, viscous model	R^2 value, viscous model	Approximating line equation, viscoelastic model	R^2 value, viscoelastic model
5.0	100	$0.119 \cdot x + 1.209$	0.998	$0.081 \cdot x + 0.799$	1.000
	350	$0.071 \cdot x + 1.265$;	0.975	$0.080 \cdot x + 0.779$	1.000
	600	$0.033 \cdot x + 1.297$	0.914	$0.072 \cdot x + 0.779$	0.987
	800	$0.027 \cdot x + 1.286$	0.985	$0.060 \cdot x + 0.776$	0.987
4.5	100	$0.119 \cdot x + 1.222$	0.999	$0.088 \cdot x + 0.904$	0.967
	350	$0.104 \cdot x + 1.216$	0.999	$0.076 \cdot x + 0.896$	0.969
	600	$0.083 \cdot x + 1.256$	1.000	$0.076 \cdot x + 0.868$	0.901
	800	$0.061 \cdot x + 1.303$	0.990	$0.064 \cdot x + 0.880$	0.874
4.0	100	$0.146 \cdot x + 1.316$	0.975	$0.120 \cdot x + 0.901$	1.000
	350	$0.126 \cdot x + 1.318$	0.987	$0.128 \cdot x + 0.860$	0.996
	600	$0.118 \cdot x + 1.294$	0.976	$0.112 \cdot x + 0.868$	0.942
	800	$0.111 \cdot x + 1.269$	0.985	$0.076 \cdot x + 0.908$	0.901
3.5	100	$0.225 \cdot x + 1.296$	0.989	$0.124 \cdot x + 1.001$	0.989
	350	$0.167 \cdot x + 1.369$	0.982	$0.132 \cdot x + 1.001$	0.983
	600	$0.090 \cdot x + 1.501$	0.939	$0.116 \cdot x + 0.977$	0.987
	800	$0.081 \cdot x + 1.527$	0.918	$0.108 \cdot x + 0.949$	0.975
3.0	100	$0.239 \cdot x + 1.415$	0.985	$0.152 \cdot x + 1.053$	0.997
	350	$0.205 \cdot x + 1.440$	0.976	$0.140 \cdot x + 1.081$	0.972
	600	$0.143 \cdot x + 1.545$	0.965	$0.144 \cdot x + 1.041$	0.973
	800	$0.099 \cdot x + 1.624$	0.975	$0.120 \cdot x + 1.073$	0.987
2.5	100	$0.227 \cdot x + 1.693$	0.969	$0.228 \cdot x + 1.049$	0.994
	350	$0.183 \cdot x + 1.731$	0.944	$0.188 \cdot x + 1.129$	0.991
	600	$0.194 \cdot x + 1.670$	0.958	$0.184 \cdot x + 1.121$	0.983
	800	$0.176 \cdot x + 1.685$	0.959	$0.150 \cdot x + 1.191$	0.977
2.0	100	$0.246 \cdot x + 1.925$	0.982	$0.276 \cdot x + 1.113$	0.994
	350	$0.221 \cdot x + 1.929$	0.975	$0.248 \cdot x + 1.276$	0.988
	600	$0.265 \cdot x + 1.839$	0.979	$0.244 \cdot x + 1.249$	0.982
	800	$0.216 \cdot x + 1.900$	0.968	$0.218 \cdot x + 1.235$	0.974
1.5	100	$0.370 \cdot x + 2.010$	0.970	$0.293 \cdot x + 1.372$	0.989
	350	$0.318 \cdot x + 2.113$	0.953	$0.309 \cdot x + 1.424$	0.985
	600	$0.350 \cdot x + 2.043$	0.975	$0.249 \cdot x + 1.568$	0.974
	800	$0.293 \cdot x + 2.165$	0.966	$0.249 \cdot x + 1.532$	0.993
1.0	100	$0.421 \cdot x + 2.628$	0.966	$0.492 \cdot x + 1.381$	0.999
	350	$0.333 \cdot x + 2.865$	0.986	$0.456 \cdot x + 1.618$	0.997
	600	$0.429 \cdot x + 2.565$	0.987	$0.380 \cdot x + 1.838$	0.991
	800	$0.391 \cdot x + 2.762$	0.994	$0.384 \cdot x + 1.778$	0.988
0.5	100	$1.002 \cdot x + 2.789$	0.911	$0.633 \cdot x + 1.705$	0.995
	350	$0.930 \cdot x + 3.055$	0.951	$0.709 \cdot x + 2.021$	0.989
	600	$0.906 \cdot x + 3.271$	0.912	$0.725 \cdot x + 2.181$	0.984
	800	$0.827 \cdot x + 3.549$	0.902	$0.685 \cdot x + 2.301$	0.975

0.1	100	$2.698 \cdot x + 2.020$	1.000	$1.021 \cdot x + 1.717$	0.999
	350	$2.731 \cdot x + 3.276$	0.997	$1.465 \cdot x + 1.950$	1.000
	600	$2.673 \cdot x + 4.187$	0.991	$1.565 \cdot x + 2.691$	0.999
	800	$2.583 \cdot x + 5.715$	0.969	$1.601 \cdot x + 2.827$	0.999
0.05	100	$3.41 \cdot x + 1.707$	1.000	$1.117 \cdot x + 1.838$	0.993
	350	$3.891 \cdot x + 2.764$	0.997	$1.690 \cdot x + 2.021$	0.999
	600	$3.983 \cdot x + 3.644$	0.987	$1.982 \cdot x + 2.518$	0.999
	800	$4.510 \cdot x + 4.792$	0.978	$2.026 \cdot x + 2.418$	0.998

S.9. Modifications in modeled grounding zones resulting from input parameters changes

Differences in grounding zone widths for the thickest and thinnest modeled glaciers for every inflow speed and every bedrock slope for both models are provided in Table S6.

Table S6. Grounding zone width difference (in meters) for a 2500 m-thick glacier and a 1000 m-thick glacier.

$\Delta GZ = GZ_{H=2.5km} - GZ_{H=1.0km}, m$ (viscous model)												
Speed, m/year	**Bed slope, %**											
	5.0	**4.5**	**4.0**	**3.5**	**3.0**	**2.5**	**2.0**	**1.5**	**1.0**	**0.5**	**0.1**	**0.05**
100	175	175	200	360	390	375	385	635	740	1866	4091	5066
350	120	160	170	265	350	320	370	550	545	1651	4266	6127
600	60	125	155	145	240	315	430	575	715	1696	4281	6627
800	35	85	150	145	135	270	370	510	615	1565	4412	6701
Mean	**98**	**136**	**169**	**229**	**279**	**320**	**389**	**568**	**654**	**1695**	**4263**	**6130**
$\Delta GZ = GZ_{H=2.5km} - GZ_{H=1.0km}, m$ (viscoelastic model)												
Speed, m/year	**Bed slope, %**											
	5.0	**4.5**	**4.0**	**3.5**	**3.0**	**2.5**	**2.0**	**1.5**	**1.0**	**0.5**	**0.1**	**0.05**
100	121	141	180	200	240	360	440	481	761	961	1502	1521
350	120	121	201	220	240	300	400	501	720	1141	2222	2543
600	100	141	201	180	240	300	400	421	600	1202	2362	2963
800	80	121	141	180	200	260	370	401	620	1142	2482	3143
Mean	**105**	**131**	**181**	**195**	**230**	**305**	**403**	**451**	**675**	**1112**	**2142**	**2543**

S.10. Modeled grounding zones

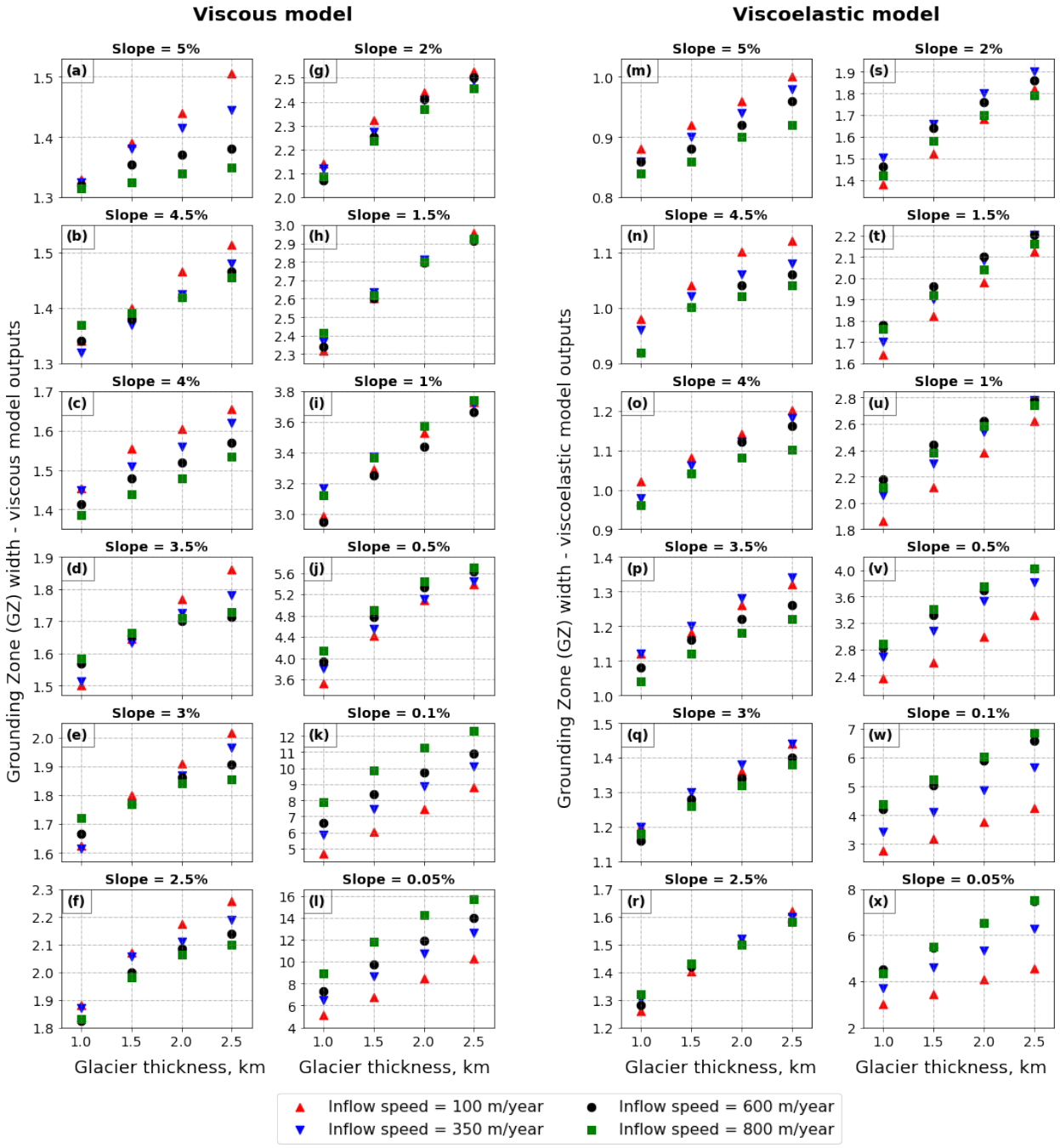

Figure S4. Dependence of the grounding zone width from the glacier thickness for all considered inflow speeds and bed slopes for both viscous and viscoelastic models. Subplots (a) – (l) correspond to the viscous model; subplots (m) – (x) correspond to the viscoelastic model. Corresponding bed slope is written above each subplot, the x-axis of each subplot shows the glacier thickness in meters, while the y-axis shows the evolution of the grounding zone as the glacier becomes thicker. Each subplot contains four sets of values, colored based on the inflow speed used as a model input at a corresponding model run.

S.11. Performance of the models

The models' accuracy is calculated as the percentage of DInSAR measurements that fall inside the model domain and is summarized in Table S7**Error! Reference source not found.**.

Table S7. Analysis of the performance of the models. The percentages shown in the table indicate the percentage of the measurements for each glacier that fall within the domain of the corresponding model.

	TOT		**REN**		**MU**	
Number of profiles	17		19		33	
Model	**Viscous**	**Viscoelastic**	**Viscous**	**Viscoelastic**	**Viscous**	**Viscoelastic**
All profiles (no error bars)	29%	88%	0%	90%	9%	82%
All profiles (with error bars)	65%	88%	47%	100%	82%	100%